

# Reconciling solvent effects on rotamer populations in carbohydrates — A joint MD and NMR analysis<sup>1</sup>

Jorge Gonzalez-Outeiriño, Karl N. Kirschner, Smita Thobhani, and Robert J. Woods

**Abstract:** The rotational preferences of the hydroxymethyl group in pyranosides is known to depend on the local environment, whether in solid, solution, or gas phase. By combining molecular dynamics (MD) simulations with NMR spectroscopy the rotational preferences for the  $\omega$  angle in methyl 2,3-di-*O*-methyl- $\alpha$ -D-glucopyranoside (**3**) and methyl 2,3-di-*O*-methyl- $\alpha$ -D-galactopyranoside (**6**) in a variety of solvents, with polarities ranging from 80 to 2.3 D have been determined. The effects of solvent polarity on intramolecular hydrogen bonding have been identified and quantified. In water, the internal hydrogen bonding networks are disrupted by competition with hydrogen bonds to the solvent. When the internal hydrogen bonds are differentially disrupted, the rotamer populations associated with the  $\omega$  angle may be altered. In the case of **3** in water, the preferential disruption of the interaction between HO6 and O4 destabilizes the *tg* rotamer, leading to the observed preference for *gauche* rotamers. Without the hydrogen bond enhancement offered by a low polarity environment, both **3** and **6** display rotamer populations that are consistent with expectations based on the minimization of repulsive intramolecular oxygen–oxygen interactions. In a low polarity environment, HO6 prefers to interact with O4, however, in water these interactions are markedly weakened, indicating that HO6 acts as a hydrogen bond donor to water.

**Key words:** carbohydrate, rotamer, molecular dynamics simulation, MD, NMR.

**Résumé :** Il est bien connu que les préférences rotationnelles des groupes hydroxyméthyles des pyranosides dépend de l'environnement local que ce soit à l'état solide, en solution ou en phase gazeuse. En combinant des simulations de dynamique moléculaire (DM) avec la spectroscopie RMN, on a pu déterminer les préférences rotationnelles pour l'angle  $\omega$  du 2,3-di-*O*-méthyl- $\alpha$ -D-glucopyranoside de méthyle (**3**) 2,3-di-*O*-méthyl- $\alpha$ -D-galactopyranoside de méthyle (**6**), dans une variété de solvants dont les polarités s'étalent de 80 à 2,3 D. On a identifié et quantifié les effets de polarité du solvant sur la liaison hydrogène intramoléculaire. Dans l'eau, la liaison hydrogène interne est perturbée par la compétition avec les liaisons hydrogènes vers le solvant. Lorsque les liaisons hydrogènes internes sont perturbées de façons différentes, les populations de rotamères associées à l'angle  $\omega$  peuvent être modifiées. Dans le cas du composé **3**, l'eau provoque une perturbation préférentielle de l'interaction entre le OH en position 6 et l'oxygène en 4 qui déstabilise le rotamère *tg*, ce qui conduit à une observation préférentielle des rotamères gauches. Lorsqu'ils ne présentent pas d'augmentation de la liaison hydrogène en raison d'un environnement de faible polarité, les populations de rotamères des composés **3** et **6** sont en accord avec ce qu'on pourrait attendre sur la base d'une minimisation des interactions répulsives oxygène–oxygène intramoléculaires. Dans un environnement de faible polarité, le OH en position 6 préfère l'interaction avec l'oxygène en 4; toutefois, dans l'eau, ces interactions sont de beaucoup affaiblies ce qui indique que le OH en position 6 agit comme donneur de liaison hydrogène pour l'eau.

**Mots clés :** hydrate de carbone, rotamère, simulation de dynamique moléculaire, DM, RMN.

[Traduit par la Rédaction]

## Introduction

The importance of understanding the relationships between conformation and biological and chemical function in carbohydrates has come to the forefront of glycobiology as

oligo- and poly-saccharides are increasingly implicated in both the healthy growth and functioning of organisms, as well as in a diverse range of disease states (1–3). Further, the covalent attachment of carbohydrates to proteins may affect both protein stability and structure (4–7), as well as,

Received 18 August 2005. Published on the NRC Research Press Web site at <http://canjchem.nrc.ca> on 5 May 2006.

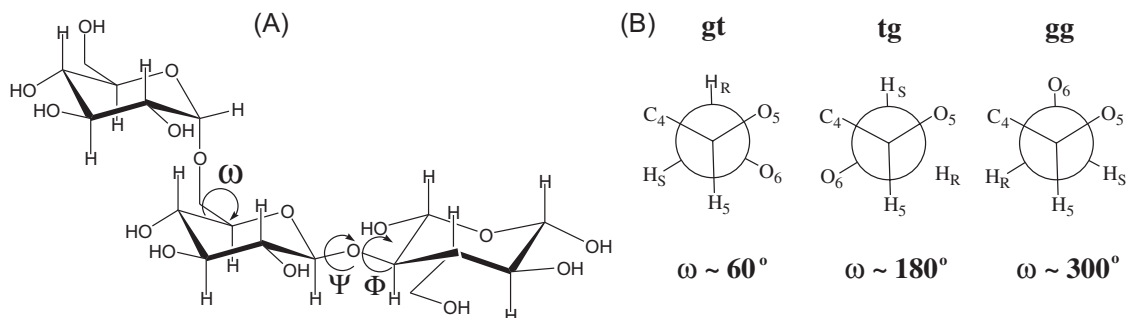
*This manuscript is dedicated to Professor Walter A. Szarek.*

**J. Gonzalez-Outeiriño, K.N. Kirschner, S. Thobhani, and R.J. Woods.**<sup>2</sup> Complex Carbohydrate Research Center, University of Georgia, 315 Riverbend Road, Athens, GA 30602, USA.

<sup>1</sup>This article is part of a Special Issue dedicated to Professor Walter A. Szarek.

<sup>2</sup>Corresponding author (e-mail: [rwoods@ccrc.uga.edu](mailto:rwoods@ccrc.uga.edu)).

**Fig. 1.** (A) Schematic diagram indicating glycosidic torsion angles in carbohydrates. (B) Nomenclature for the  $\omega$  torsion angle (O6-C6-C5-O5). Qualitatively, the three staggered rotamers are commonly defined with respect to the O6-C6-C5-O5 and O6-C6-C5-C4 torsion angles as gauche-gauche (*gg*), gauche-trans (*gt*), and trans-gauche (*tg*).



conversely, function (8–10). The ability to correlate biological function with glycan structure can provide not only mechanistic insight (11), but is also of benefit in optimizing carbohydrate-based therapeutic agents (12).

X-ray crystallography, NMR spectroscopy, and theoretical calculations are the three techniques most commonly used in the conformational analysis of carbohydrates. X-ray crystallography has been very successful in characterizing protein-carbohydrate complexes, provided that the carbohydrate is limited in size (13, 14). However, single crystal X-ray diffraction structures of oligo- and poly-saccharides are extremely rare; a direct result of difficulties in crystallizing the generally flexible oligosaccharides (15). For solution conformational analysis, NMR spectroscopy is the preferred technique. However, the deconvolution of the observed NMR properties, such as chemical shifts, scalar  $J$  couplings, nuclear Overhauser effects (NOEs), and residual dipolar couplings, into the 3-D structures that are present in solution presents particular difficulties for these flexible molecules (16, 17). The challenge in deriving a mixture of physically real conformations from a spectroscopic signal that arises from the average of the conformational ensemble is generally met by introducing some aspect of theoretical modeling into the NMR data analysis. Unlike the situation with protein structure determinations by NMR, the use of NMR observables as restraints during the modeling of flexible carbohydrates can lead to the generation of nonphysical virtual conformations (18). To avoid this problem, theoretical calculations are generally employed in one of two ways, either to provide discrete models for the presumed conformations present in solution or to independently predict the conformational states. In the former application, a limited number of theoretical structures are generated, usually by some form of gas-phase energy minimization (quantum or classical mechanical energies) of initial conformations. Based on the computed NMR properties for each individual structure it may then be possible to establish the populations of the individual structures that give the best agreement with experiment. Perhaps the most significant limitation to the accuracy of this approach is the selection of the individual structures, which is often based on scientific intuition. In contrast, molecular dynamics (MD) simulations or Monte Carlo sampling may be employed to predict the ensemble of conformations that the carbohydrate populates at room temperature in the appropriate solvent, independent of investigator bias (19). The accuracy of this latter approach is limited by the

choice of classical mechanical force field. Force field development remains an active research area; however, MD simulations are generally able to accurately identify the conformational states present in solution and can often predict their populations with reasonably accuracy (20–24, 19).

In solution, 3-D structures of oligosaccharides have been shown to exist as an equilibrium among several conformations, owing to the flexibility introduced in the structure by the glycosidic linkages,  $\Phi$ ,  $\Psi$ , and  $\omega$  (see Fig. 1). The conformations of the first two torsion angles ( $\Phi$ ,  $\Psi$ ) are dominated mainly by stereoelectronic (anomeric effect) and steric effects (25, 26). As would be expected for an ether-type linkage, the  $\omega$  torsion angle may adopt any of the three staggered rotamers, with populations depending heavily on the configuration at C4 and on the polarity of the local environment (27, 23).

In the solid state, an early report based on a statistical analysis of X-ray structures (28) revealed two remarkably different conformational behaviors for the  $\omega$  torsion angle in carbohydrates. The glucopyranosides and mannopyranosides showed clear preferences for only the *gg* and *gt* conformations, with ratios of approximately 40:0:60 (*gt:tg:gg*), while galactopyranosides showed a significant population of the *tg* rotamer, with a ratio of approximately 58:34:8 (*gt:tg:gg*). Similar trends have been inferred from NMR data in aqueous solution for both the glucopyranosyl (50:0:53 (29), 38:4:58 (30), 44.7:3.5:51.8 (31), and 52:7:41 (32)) and galactopyranosyl series (56:32:12 (29), 61:21:18 (30), 71.6:13.9:14.5 (31), 65:21:14 (33), and 67:30:3(32)). A detailed review of the conformational properties of the  $\omega$  angle has been provided by Bock and Duus (29).

In contrast to the condensed-phase experimental data, gas-phase quantum mechanical calculations fail to predict the correct rotamer populations unless the formation of internal hydrogen bonds among hydroxyl groups at C4 and C6 or between the hydroxyl group at C6 and the ring oxygen atom is prevented (34, 23, 31). A Boltzman analysis of the gas-phase quantum mechanical energies, computed at the B3LYP/6-31G(2d,2p) level has been performed for methyl  $\alpha$ -D-glucopyranosides and galactopyranosides. A theoretical population ratio of 43:29:28 was obtained for the glucopyranoside when internal hydrogen bonding was allowed, whereas qualitative agreement with experiment (62:0:37) was only obtained when intramolecular hydrogen bonds were prevented from forming. Similarly for the galactopyranoside, ratios of 38:5:57 (with internal hydrogen bonds)

and 41:59:0 (without) were obtained (23). In neither derivative were the gas-phase calculations able to give quantitative agreement with experiment, although they suggested a role for internal hydrogen bonding. It should be noted that in all structures examined quantum mechanically, prevention of internal hydrogen bonding led to significantly higher energies relative to those of conformations in which intramolecular hydrogen bonds were present (23). Nonetheless, the observation that qualitative agreement with experiment was obtained only in the absence of intramolecular hydrogen bonds is consistent with an interpretation of rotamer populations as arising from the minimization of unfavorable 1,3-diaxial electrostatic interactions among O4, O5, and O6 (29, 23).

To obtain quantitative agreement between theoretical calculations and experiment, it was found necessary to include water explicitly in the MD simulations of the glucopyranosides and galactopyranosides (23). The mechanism whereby solvent influences  $\omega$  population in methyl  $\alpha$ -D-glucopyranoside has previously been examined experimentally in an NMR analysis of the 2,3,4,6-tetra- and 2,3,4-tri-*O*-methylated derivatives in several solvents (27). By examining the effect of solvent polarity on rotamer population of these methylated derivatives, Rockwell and Grindley (27) made two important observations, namely that permethylation removed any dependence of rotamer population on solvent polarity (maintaining approximately a ratio of 61:38:0), and, in contrast, that when O6 was unsubstituted there was a strong dependence on polarity. They inferred that polar solvents led to a decrease of intramolecular hydrogen bonding, but also that hydrogen bond donation from the hydroxymethyl group to water was not important in determining rotational preferences.

Here we extend the work of Rockwell and Grindley to derivatives of both glucopyranosides and galactopyranosides in which we elected to examine derivatives that, like the natural carbohydrates, have free hydroxyl groups at either O4 or O6. Thus, we have synthesized methyl 2,3-di-*O*-methyl- $\alpha$ -D-glucopyranoside (**3**) and methyl 2,3-di-*O*-methyl- $\alpha$ -D-galactopyranoside (**6**), and determined the rotational properties of each of their  $\omega$  angles by NMR in a variety of solvents. By employing these simple models, an assessment of the importance of hydrogen bond donation from HO4 to O6 may be made, as well as of the effect of configuration at C4 on rotamer population as a function of solvent polarity. In addition, a detailed examination of the hydrogen bond properties for these glycosides and related disaccharides was undertaken by performing the longest explicitly solvated MD simulations reported to date in both water and dichloromethane. Data from the theoretical simulations is used to provide atomic level insight into the validity of the inferences made on the basis of the experimental data.

## Experimental

### General

$^1\text{H}$  and  $^{13}\text{C}$  NMR and 2-D correlation spectra were recorded on Varian 300 and 500 MHz spectrometers, each equipped with Sun off-line editing workstations. Chemical shifts were measured in parts per million ( $\delta$ ) relative to the appropriate solvent peaks and the scalar coupling constants

(*J*) were measured in Hertz (Hz). Matrix assisted laser desorption ionization – time-of-flight (MALDI-TOF) mass spectra were recorded using a Hewlett Packard G2025A system with 2,5-dihydroxybenzoic acid (gentisic acid) (10 mg/mL in 50% acetonitrile) as the matrix. Melting points were recorded on a Kofler hot stage apparatus and are uncorrected.

Chemicals and reagents were purchased from Sigma-Aldrich, Fluka, or VWR and used without further purification unless otherwise stated. The reaction solvent (acetonitrile) was distilled from calcium hydride and stored over 4 Å molecular sieves prior to use. Ethanol was used without any further purification.

## Synthesis

### Methyl 4,6-*O*-benzylidene- $\alpha$ -D-glucopyranoside (**1**)

To a solution of methyl  $\alpha$ -D-galactopyranoside (2.11 g, 10.87 mmol) in dry acetonitrile (60 mL) was added benzaldehyde dimethyl acetal (2.80 g, 18.40 mmol) and the solution acidified with camphorsulfonic acid (approx. 0.05 g, 0.22 mmol) to pH 3. After stirring at room temperature under an atmosphere of argon for 15 h, the mixture was neutralized with triethylamine and concentrated in vacuo to dryness using toluene as a cosolvent. The resulting residue was recrystallized from ethyl acetate – hexane to afford compound **1** as a white crystalline solid (2.22 g, 76%); mp 165–167 °C (lit. value (35) mp 166 to 167 °C).  $^1\text{H}$  NMR (300 MHz,  $\text{CDCl}_3$ )  $\delta$ : 7.53–7.45 (m, 2H, Ph), 7.41–7.33 (m, 3H, Ph), 5.53 (s, 1H, PhCH), 4.80 (d, 1H, H1), 4.30 (dd, 1H, H6a), 3.93 (t, 1H, H3), 3.85–3.77 (m, 1H, H5), 3.73 (t, 1H, H6b), 3.63 (dd, 1H, H2), 3.49 (t, 1H, H4), 3.46 (s, 3H,  $\text{OCH}_3$ ).  $^{13}\text{C}$  NMR (75 MHz,  $\text{CDCl}_3$ )  $\delta$ : not observed (Cq, Ph), 129.2, 126.7 (5  $\times$  Ph), 101.7 (PhCH), 99.2 (C1), 81.7 (C4), 72.9 (C2), 71.7 (C3), 69.2 (C6), 62.9 (C5), 55.4 ( $\text{OCH}_3$ ). MALDI-TOF MS *m/z*: 305.2 [ $\text{M} + \text{Na}$ ] $^+$ .

### Methyl 4,6-*O*-benzylidene-2,3-di-*O*-methyl- $\alpha$ -D-glucopyranoside (**2**)

Methyl 4,6-*O*-benzylidene- $\alpha$ -D-glucopyranoside (500 mg, 1.77 mmol) was dissolved in dry DMF (20 mL) under a nitrogen atmosphere. To this was added 60% NaH suspended in oil (260 mg, 6.50 mmol) followed by the dropwise addition of methyl iodide (340  $\mu\text{L}$ , 5.46 mmol) and the reaction was left to stir for 16 h under a nitrogen atmosphere at room temperature. After this time, the reaction was quenched with water (40 mL) and the aqueous layer was washed with ethyl acetate (3  $\times$  50 mL). The combined organic layers were then washed with satd.  $\text{NaHCO}_3$  (3  $\times$  50 mL) and water (3  $\times$  50 mL). The combined organic layers were dried ( $\text{MgSO}_4$ ), filtered, and the solvent removed in vacuo and the residue recrystallized from ethanol to furnish **2** as a white solid (270 mg, 49%); mp 121 to 122 °C (lit. value (36) mp 122 to 123 °C).  $^1\text{H}$  NMR (300 MHz,  $\text{CDCl}_3$ )  $\delta$ : 7.53–7.45 (m, 2H, Ph), 7.40–7.31 (m, 3H, Ph), 5.54 (s, 1H, PhCH), 4.85 (d, 1H, H1), 4.28 (dd, 1H, H6a), 3.88–3.78 (m, 1H, H5), 3.74 (dd, 1H, H6b), 3.69 (t, 1H, H3), 3.64 (s, 3H,  $\text{OCH}_3$ ), 3.56 (s, 3H,  $\text{OCH}_3$ ), 3.53 (t, 1H, H4), 3.45 (s, 3H,  $\text{OCH}_3$ ), 3.30 (t, 1H, H2).  $^{13}\text{C}$  NMR (75 MHz,  $\text{CDCl}_3$ )  $\delta$ : not observed (Cq, Ph), 129.4, 126.9 (5  $\times$  Ph), 101.9 (PhCH), 98.1 (C1), 81.9

(C2), 81.9 (C4), 80.6 (C3), 69.4 (C6), 61.9 (C5), 60.6, 59.4, 55.6 (3 × OCH<sub>3</sub>). MALDI-TOF MS *m/z*: 332.8 [M + Na]<sup>+</sup>.

#### Methyl 2,3-di-O-methyl- $\alpha$ -D-glucopyranoside (3)

To methyl 4,6-*O*-benzylidene-2,3-di-*O*-methyl- $\alpha$ -D-glucopyranoside (250 mg, 0.81 mmol) was added a solution of 80% acetic acid in water (15 mL) and the mixture was heated to 50 °C. After a period of 4 h, the reaction mixture was cooled, concentrated in vacuo, and then coevaporated with toluene (3 × 20 mL). The residue was recrystallized from ethyl acetate – hexane to give the desired compound **3** as a white solid (73 mg, 41%); mp 81–84 °C (lit. value (37) mp 84 °C). <sup>1</sup>H NMR (500 MHz, CDCl<sub>3</sub>)  $\delta$ : 4.84 (d, 1H, H1), 3.85 (dd, 1H, H6a), 3.80 (dd, 1H, H6b), 3.65–3.61 (m, 1H, H5), 3.63 (s, 3H, OCH<sub>3</sub>), 3.49 (s, 3H, OCH<sub>3</sub>), 3.50 (dd, 1H, H4), 3.43 (s, 3H, OCH<sub>3</sub>), 3.46 (dd, 1H, H3), 3.21 (dd, 1H, H2). <sup>13</sup>C NMR (75 MHz, D<sub>2</sub>O)  $\delta$ : 97.3 (C1), 83.0 (C3), 80.6 (C2), 72.2 (C5), 69.8 (C4), 61.2 (C6), 60.6, 58.5, 55.4 (3 × OCH<sub>3</sub>). MALDI TOF *m/z*: 245.2 [M + Na]<sup>+</sup>.

#### Methyl 4,6-O-benzylidene- $\alpha$ -D-galactopyranoside (4)

The synthesis of methyl 4,6-*O*-benzylidene- $\alpha$ -D-galactopyranoside was carried out following the procedure described for the preparation of the methyl 4,6-*O*-benzylidene- $\alpha$ -D-glucopyranoside. Thus, methyl  $\alpha$ -D-galactopyranoside (1.00 g, 5.15 mmol) in dry acetonitrile (160 mL) was reacted with benzaldehyde dimethyl acetal (2.20 g, 14.45 mmol) and camphorsulfonic acid (approx. 0.03 g, 0.13 mmol) to afford **4** as a white crystalline solid after recrystallization (0.73 g, 50%); mp 169–171 °C (lit. value (35) mp 168 to 169 °C). <sup>1</sup>H NMR (300 MHz, CDCl<sub>3</sub>)  $\delta$ : 7.52–7.35 (m, 5H, Ph), 5.55 (s, 1H, PhCH), 4.92 (d, 1H, H1), 4.28 (dd, 1H, H6a), 4.25 (dd, 1H, H4), 4.08 (dd, 1H, H6b), 3.93 (dd, 1H, H2), 3.89 (dd, 1H, H3), 3.69 (ddd, 1H, H5), 3.46 (s, 3H, OCH<sub>3</sub>). <sup>13</sup>C NMR (75 MHz, CDCl<sub>3</sub>)  $\delta$ : not observed (Cq, Ph), 129.4, 128.2, 126.3 (5 × Ph), 101.3 (PhCH), 100.0 (C1), 75.7 (C4), 70.0 (C2), 70.0 (C3), 69.4 (C6), 62.5 (C5), 55.7 (OCH<sub>3</sub>). MALDI-TOF MS *m/z*: 305.1 [M + Na]<sup>+</sup>.

#### Methyl 4,6-O-benzylidene-2,3-di-O-methyl- $\alpha$ -D-galactopyranoside (5)

The synthesis of methyl 4,6-*O*-benzylidene-2,3-di-*O*-methyl- $\alpha$ -D-galactopyranoside was carried out following the procedure described for the preparation of the methyl 4,6-*O*-benzylidene-2,3-di-*O*-methyl- $\alpha$ -D-glucopyranoside. Thus, methyl 4,6-*O*-benzylidene- $\alpha$ -D-galactopyranoside (700 mg, 2.48 mmol) was reacted with NaH (300 mg, 7.50 mmol) and methyl iodide (900  $\mu$ L, 14.46 mmol) in dry DMF (20 mL) to give **5** as a white solid after recrystallization (230 mg, 40%); mp 126 to 127 °C (lit. value (38) mp 127 to 128 °C). <sup>1</sup>H NMR (300 MHz, CDCl<sub>3</sub>)  $\delta$ : 7.56–7.48 (m, 2H, Ph), 7.38–7.29 (m, 3H, Ph), 5.53 (s, 1H, PhCH), 4.97 (d, 1H, H1), 4.30 (d, 1H, H4), 4.22 (d, 1H, H6a), 4.03 (d, 1H, H6b), 3.77 (dd, 1H, H2), 3.66 (dd, 1H, H3), 3.57 (s, 1H, H5), 3.51 (s, 3H, OCH<sub>3</sub>), 3.50 (s, 3H, OCH<sub>3</sub>), 3.43 (s, 3H, OCH<sub>3</sub>). <sup>13</sup>C NMR (75 MHz, CDCl<sub>3</sub>)  $\delta$ : 137.9 (Cq, Ph), 128.9, 128.1, 126.3 (5 × Ph), 101.1 (PhCH), 98.5 (C1), 77.6 (C2), 77.6 (C3), 73.7 (C4), 69.4 (C6), 62.5 (C5), 59.0, 57.8, 55.4 (3 × OCH<sub>3</sub>). MALDI-TOF MS *m/z*: 332.8 [M + Na]<sup>+</sup>.

#### Methyl 2,3-di-O-methyl- $\alpha$ -D-galactopyranoside (6)

The synthesis of methyl 2,3-di-*O*-methyl- $\alpha$ -D-galactopyranoside was carried out following the procedure described for the preparation of the methyl 2,3-di-*O*-methyl- $\alpha$ -D-glucopyranoside. Thus, methyl 4,6-*O*-benzylidene-2,3-di-*O*-methyl- $\alpha$ -D-galactopyranoside (230 mg, 0.74 mmol) was treated with 80% acetic acid (15 mL) to give the desired product **6** as a white solid after recrystallization (49 mg, 30%). <sup>1</sup>H NMR (500 MHz, CDCl<sub>3</sub>)  $\delta$ : 4.90 (d, 1H, H1), 4.13 (dd, 1H, H4), 3.94 (dd, 1H, H6a), 3.81 (dd, 1H, H6b), 3.76 (t, 1H, H5), 3.56 (dd, 1H, H2), 3.52 (dd, 1H, H3), 3.49 (s, 3H, OCH<sub>3</sub>), 3.48 (s, 3H, OCH<sub>3</sub>), 3.41 (s, 3H, OCH<sub>3</sub>), 2.01 (s, 3H, OCH<sub>3</sub>). <sup>13</sup>C NMR (75 MHz, CDCl<sub>3</sub>)  $\delta$ : 97.7 (C1), 78.9 (C3), 77.2 (C2), 69.0 (C5), 67.4 (C4), 62.5 (C6), 58.7, 57.7, 55.1 (3 × OCH<sub>3</sub>). MALDI-TOF MS *m/z*: 245.2 [M + Na]<sup>+</sup>.

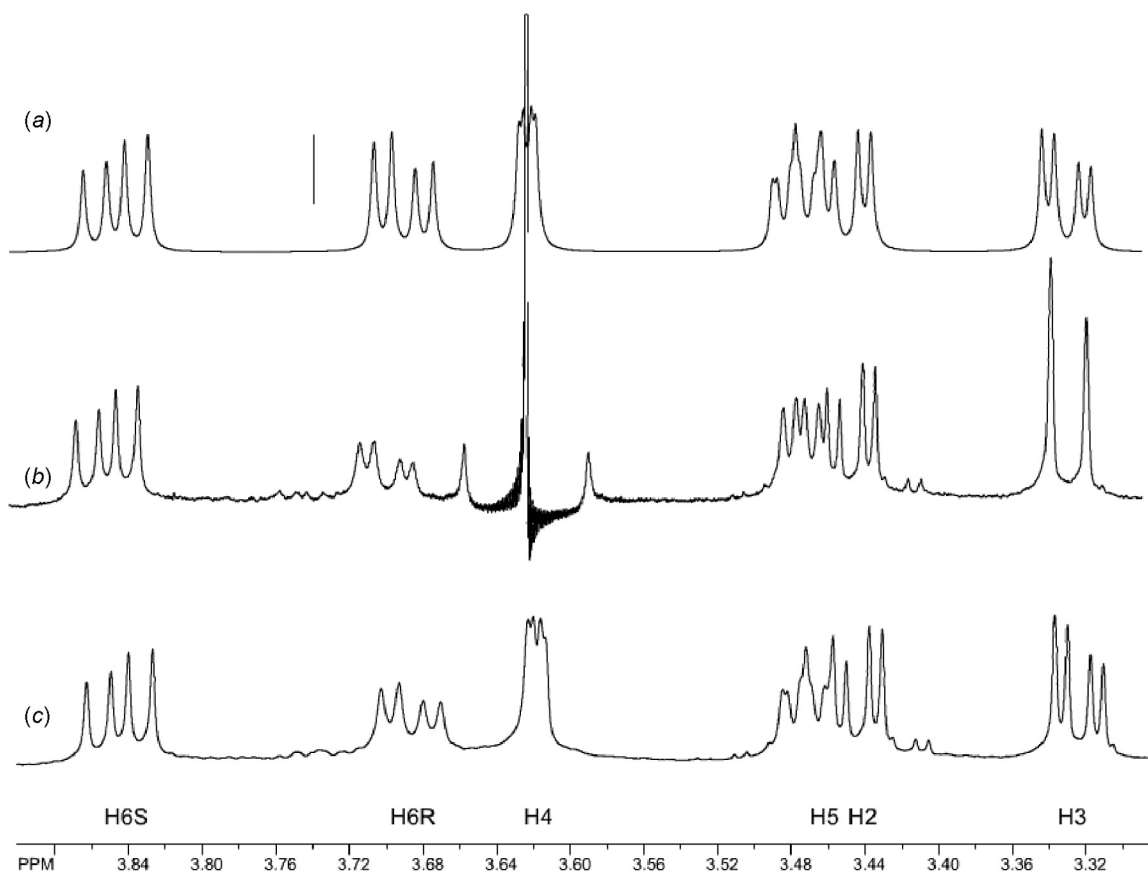
#### Molecular dynamics simulation

Molecular dynamics (MD) simulations were performed using the SANDER module in the AMBER5 program suite (39) with the GLYCAM (40) parameters for carbohydrates. The 1–4 electrostatic and van der Waals interactions were unscaled (SCEE = 1.0 and SCNB = 1.0), in contrast to the traditional AMBER formalism, but as demonstrated to be essential for carbohydrate simulations (23). The MD simulations were performed using an nPT ensemble with TIP3P water (41) and a dielectric constant set to unity. A long range cutoff of 8 Å was employed. For solvation in water, the carbohydrates were immersed in a theoretical box of 484 (**3**) and 473 (**6**) water molecules with approximate dimensions of 28 Å × 27 Å × 23 Å. For simulations employing dichloromethane, a cutoff of 12 Å was employed with a slightly larger theoretical box (34 Å × 32 Å × 29 Å) of 294 dichloromethane molecules (42) for both carbohydrates. The SHAKE algorithm was applied to all hydrogen-containing bonds, using the default settings. Initial conjugate-gradient energy minimization (20 000 cycles), with restrained solute coordinates, was performed on all systems studied, employing a 0.01 kcal mol<sup>-1</sup> Å (1 cal = 4.184 J) convergence criterion in the energy gradient. Subsequently, energy minimization of the entire system was performed followed by a simulated annealing period for the solvent, during which the systems were heated from 5 to 300 K for a period of 50 ps, held at 300 K for 250 ps in the case of water, and 1350 ps in dichloromethane, and then the systems were cooled to 5 K over 50 ps. Lastly, the systems were heated from 5 to 300 K over 50 ps prior to the production run MD simulations. Between 100–120 ns of data were collected for each system at 300 K. In all simulations, a 2 fs time step was employed in the integration of the equations of motion. The extremely long MD simulation times were required to achieve adequate sampling of the rotational states. The post-simulation analyses were performed using the CARNAL module of the AMBER suite of programs.

#### NMR

Each carbohydrate (5–10 mg per sample) was dissolved in each of the different deuterated solvents (D<sub>2</sub>O, DMSO-*d*<sub>6</sub>, CD<sub>3</sub>CN, CD<sub>2</sub>Cl<sub>2</sub>, CDCl<sub>3</sub>, toluene-*d*<sub>8</sub>, benzene-*d*<sub>6</sub>) and introduced into a 5 mm NMR tube. The NMR experiments were performed on Varian 600 and 500 MHz spectrometers. One-

**Fig. 2.** Expansion of the experimental and simulated  $^1\text{H}$  NMR spectra for **6** in toluene- $d_8$ : (A) simulated spectrum; (B) homodecoupled experimental spectrum with irradiation of H4; (C) experimental spectrum.



dimensional  $^1\text{H}$  spectra and homodecoupled experiments with irradiation of the H4 and hydroxyl proton, OH6, were performed to obtain the initial  $^3J_{\text{H5-H6(R or S)}}$  couplings (Fig. 2). Final values for the scalar couplings were obtained by iterative spectral simulation using the SPINWORKS (43) and PERCH NMR software (44).

## Results and discussion

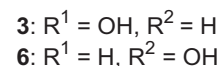
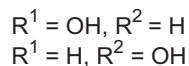
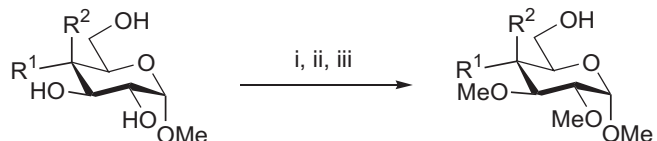
### Synthesis of methyl 2,3-di-*O*-methyl- $\alpha$ -D-glucopyranoside and galactopyranoside

The desired 2,3-di-methylated  $\alpha$ -D-glucopyranosides and galactopyranosides were prepared in three steps following established procedures (Scheme 1). Thus, regioselective benzylidenation of the commercially available methyl  $\alpha$ -pyranosides at the O4 and O6 positions, followed by methylation of the hydroxyls at the C2 and C3 positions, resulted in the fully protected intermediates (**2** and **5**). The final step involved the acid-mediated cleavage of the benzylidene acetal to give the desired compounds (**3** and **6**) as white solids after recrystallization.

### Calculation of $^3J_{\text{HH}}$ couplings

Due to the rapid rotational timescale for the  $\omega$  angle (45, 46), the rotamer population from NMR spectroscopy may only be indirectly inferred. Any experimental measurement corresponding to a fast equilibrium with respect to the timescale of the technique can be interpreted as a weighted

**Scheme 1.** Synthesis of methyl 2,3-di-*O*-methyl-pyranosides. Reaction conditions: (i)  $\text{PhCH}(\text{OMe})_2$ , CSA, MeCN; (ii) MeI, NaH, DMF, RT; (iii) 80% AcOH,  $\text{H}_2\text{O}$ , 50  $^\circ\text{C}$ .



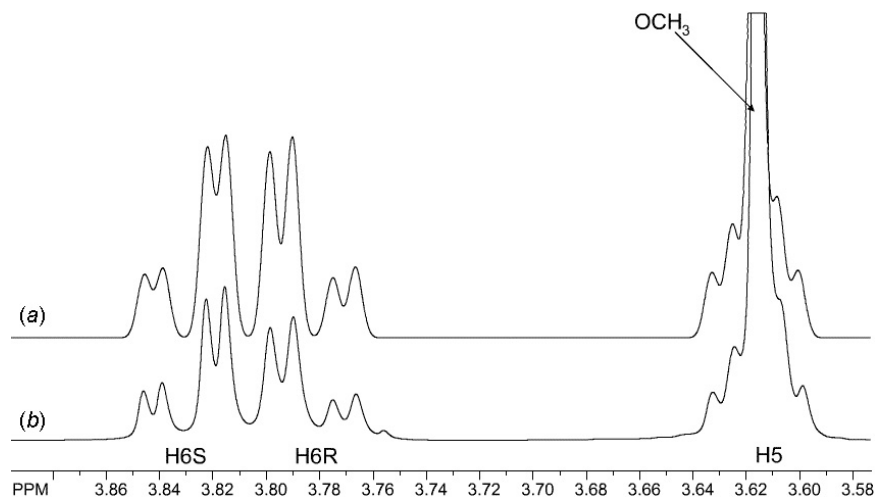
average of contributions from the individual states involved in the process. In the case of  $\omega$ -angle populations, at least three conformations should be considered as being in fast equilibrium on the NMR timescale (29, 27, 47). The NMR data for the  $^3J_{\text{HH}}$  couplings related to the C5-C6 rotational equilibrium are generally deconvoluted into rotamer populations using eqs. [1]–[3]:

$$[1] \quad ^3J_{\text{H5-H6R}} = n_{gt} ^3J_{(\text{H5-H6R}, gt)} + n_{tg} ^3J_{(\text{H5-H6R}, tg)} + n_{gg} ^3J_{(\text{H5-H6R}, gg)}$$

$$[2] \quad ^3J_{\text{H5-H6S}} = n_{gt} ^3J_{(\text{H5-H6S}, gt)} + n_{tg} ^3J_{(\text{H5-H6S}, tg)} + n_{gg} ^3J_{(\text{H5-H6S}, gg)}$$

$$[3] \quad n_{gt} + n_{tg} + n_{gg} = 1$$

**Fig. 3.** Expansion of the experimental and simulated spectra for **3** in CDCl<sub>3</sub>: (A) simulated spectrum; (B) experimental spectrum.



in which  ${}^3J_{\text{H5-H6R}}$  and  ${}^3J_{\text{H5-H6S}}$  are the experimentally measured couplings between protons H5 and each of the prochiral H6 protons, and  ${}^3J_{(\text{H5-H6}, ii)}$  are the limiting values of the specific coupling constants in each conformational state  $ii$  with population  $n_{ii}$ .

There are numerous sources of uncertainty in this approach, both in terms of the experimental measurements and in the data interpretation. Second-order effects are commonly observed in this type of spectra (Fig. 3), making the use of directly measured  ${}^3J$  values inappropriate. To remove the second-order effects, the spectra were simulated via an iterative procedure in which the first-order  ${}^3J$  couplings were varied, until optimal agreement between the experimental and the predicted spectra was achieved (43).

There are two further significant limitations of this method, related to the calculation of the  ${}^3J$  couplings. Firstly,  ${}^3J$  couplings are generally computed using a Karplus-type equation that correlates coupling constants with dihedral angles and many approaches to the parameterization of these relationships have been proposed, including empirical methods based on experimental data (48) and theoretical methods based on quantum mechanical data (32). In the case of the empirical equation reported by Haasnoot et al. (48), the equation included the effects of electronegative substituents on the  ${}^3J_{\text{HH}}$  values, but was parameterized using rigid model compounds. A single equation was developed for computing each of the  ${}^3J_{\text{H5-H6R}}$  and  ${}^3J_{\text{H5-H6S}}$  values. This approach can lead to the prediction of small negative rotamer populations, particularly for dynamic systems. The equation introduced by Stenutz et al. (32) was parameterized using  ${}^3J$  couplings computed from density functional theory (DFT) for a set of model compounds. By considering variations in the  $\omega$  conformations, as well as in the orientation of the hydroxyl groups, Stenutz et al. arrived at a separate equation for the couplings between H5 and each of the prochiral H6 protons, reflecting both geometric and electronic variations in the pro-R and pro-S environments. A promising alternative is to compute the  ${}^3J$  couplings directly from quantum mechanical calculations, without employing an empirical Karplus-type equation (49). This method has many benefits; however, its computationally intensity makes it challenging to employ when analyzing the

**Table 1.** Limiting  ${}^3J$  values employed in the present analysis.

Coupling constant	Empirically derived (48)			Quantum derived (32)		
	<i>gt</i>	<i>tg</i>	<i>gg</i>	<i>gt</i>	<i>tg</i>	<i>gg</i>
${}^3J_{\text{H5-H6R}}$	10.7	5	0.9	9.9	4.5	0.8
${}^3J_{\text{H5-H6S}}$	3.1	10.7	2.8	1.5	10.8	1.3

**Note:**  $J$  values are in Hertz.

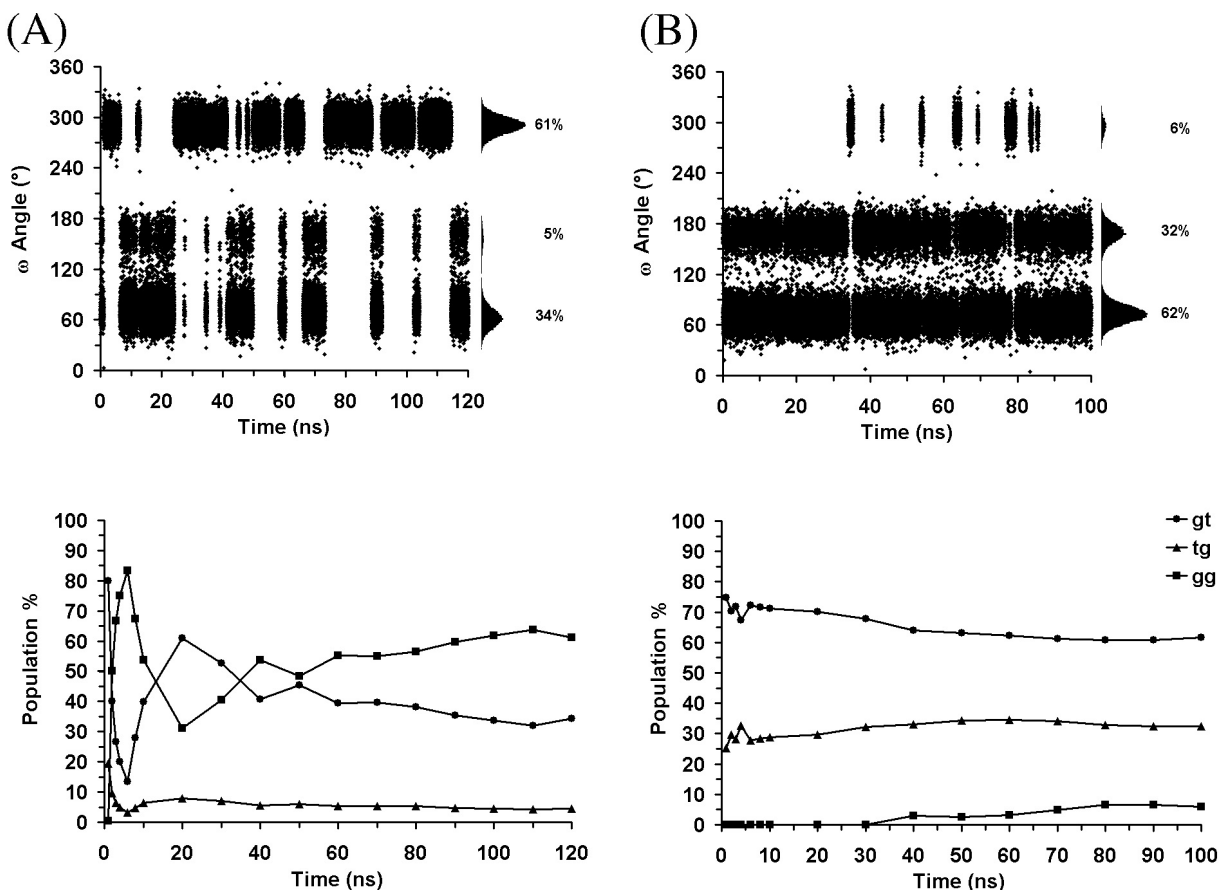
thousands of conformations typically generated during MD simulations.

In the parameterization of the any given Karplus-type relationship, a set of limiting  ${}^3J$  values must be derived for each rotamer. The accuracy of the limiting  $J$  values is critical when applying eqs. [1]–[3]. Previously, it was assumed that the  $\omega$  angle would adopt idealized values of 60°, 180°, and –60° in each of the rotameric states; however, this approach often led to small unrealistic negative rotamer populations. More recently, gas-phase energy minimized geometries have been employed for each rotamer. Notably, these optimized geometries differed markedly from idealized values (29, 27). As part of this study, the extent to which the omission of solvent in the geometry optimizations biases the conformations away from those actually present in solution will be examined. Gas-phase energy minimization always leads to an excessive degree of internal hydrogen bonding (23), which is expected to introduce some level of distortion into the  $\omega$  angle relative to its orientation in water. To assess the effect of the limiting  $J$  value on the derivation of the rotamer populations we have employed both the empirical and quantum-derived values (see Table 1).

### MD simulations

The rotamer populations of the  $\omega$  torsion angle were predicted (Fig. 4) from explicitly solvated simulations of **3** and **6** in both water and dichloromethane (see Fig. 4). It may be seen that conformational convergence for these systems was not reached until simulation times of between 40 and 80 ns. A reoccurring question when running MD simulations is, “When has a simulation been run long enough that conclu-

**Fig. 4.** MD trajectories (120 and 100 ns) of the  $\omega$  angle in (A) methyl 2,3-di-*O*-methyl- $\alpha$ -D-glucopyranoside (**3**) and (B) methyl 2,3-di-*O*-methyl- $\alpha$ -D-galactopyranoside (**6**) in water, with resulting histograms and population % on the right-hand side of each figure. Conformational convergence is plotted below the respective trajectories.



sions about the dynamic properties of a system can be drawn?" The amount of simulation time required to reach conformational equilibration will vary depending on the lifetime of the possible conformations, which itself is directly related to the barrier heights among the states. A molecule that has long conformational lifetimes, exhibiting infrequent conformation transitions, will require a long simulation time period to reach dynamic convergence. Conversely, a molecule that possesses short conformational lifetimes and frequent conformation transitions, will require a shorter simulation to reach convergence. In terms of the rotational states of the  $\omega$  angle in **3**, there are frequent transitions between the *gt* and *tg* rotamers, and infrequent transitions to the *gg* rotamer, as seen in Fig. 4. The infrequent transitions of the *gg* rotamer, coupled with the large populations of the *gt* and *gg* rotamers, resulted in the slow convergence of the *gt* and *gg* rotamers. A relatively low energy barrier between *gt* and *tg* would explain the rapid transitions, while a higher energy barrier between *tg* and *gg* is consistent with the long lifetime for each of these rotamers. These results are in qualitative agreement with the quantum mechanical rotational energy curves computed for the rotation of the  $\omega$  angle in methyl  $\alpha$ -D-glucopyranoside (23).

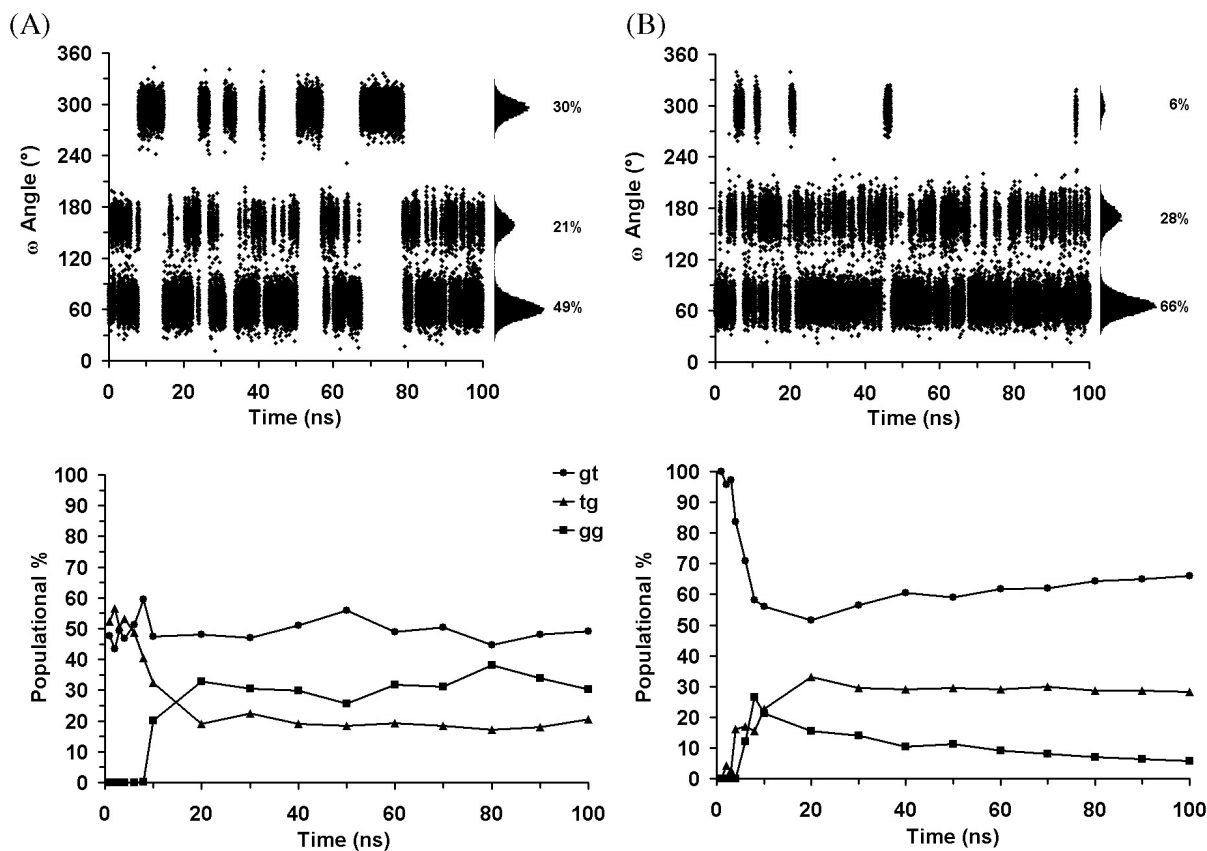
A very different behavior for rotamer interconversions was observed for **6**, displaying frequent transitions between the *gt* and *tg* rotamers, and only infrequent transitions to the

*gg* rotamer. In contrast to the case of **3**, the rotamer distribution in **6** reached convergence in less than 50 ns, with a rotamer ratio of 62:27:11. Again, in terms of rotational barriers, the frequency of transitions between the *gt* and *tg* states indicates a low energy barrier between these rotamers and high energy barriers around the *gg*. The rotamer convergence was achieved more rapidly than in **3** because the two rotamers with higher populations are in frequent transition with each other.

In water, the rotamer distributions for methyl 2,3-di-*O*-methyl- $\alpha$ -D-glucopyranosides (**3**) and methyl 2,3-di-*O*-methyl- $\alpha$ -D-galactopyranoside (**6**) were predicted to be 34:6:61 and 62:32:6, respectively, which are in reasonable agreement with the previously reported experimental data for the underivatized methyl glycosides (41:1:58 and 61:18:21, respectively) (30). The results from the present MD simulations are also similar to those from the 50 ns fully solvated MD simulations previously reported (23) for methyl  $\alpha$ -D-glucopyranoside (40:6:54) and methyl  $\alpha$ -D-galactopyranoside (64:28:8). These observations confirm that methylation of oxygens O2 and O3 does not make a remarkable impact on the rotamer population of the  $\omega$  torsion angle in either **3** or **6** in water.

In an attempt to examine the ability of MD simulations to predict the effect of solvent polarity on rotamer population, MD simulations of **3** and **6** in  $\text{CH}_2\text{Cl}_2$  were performed. It

**Fig. 5.** MD trajectories (100 ns) of the  $\omega$  angle in (A) methyl 2,3-di-*O*-methyl- $\alpha$ -D-glucopyranoside (**3**) and (B) methyl 2,3-di-*O*-methyl- $\alpha$ -D-galactopyranoside (**6**) in dichloromethane, with resulting histograms and population % on the right-hand side of each figure. Conformational convergence is plotted below the respective trajectories.



should be noted that there are at present no force field parameters available for deuterated solvents, and simulations in nonaqueous solvents are uncommon. Thus, the solvent model for  $\text{CH}_2\text{Cl}_2$  is relatively untested; however, the initial results are encouraging, particularly in the case of **3** (Fig. 5).

The simulation produced a population conformation ratio of 49:21:30 for **3**, which indicates a significant increase in the population of the *tg* and *gt* rotamers at the expense of the *gg* rotamer, relative to the system in water (34:6:61, *gt:tg:gg*). A negligible effect was predicted for **6** (66:28:6 in  $\text{CH}_2\text{Cl}_2$  vs. 64:28:8 in water); however, an examination of the convergence plots indicates that even after 100 ns the populations have not fully converged.

It is interesting to note that the  $\omega$  torsion angle displayed sensitivity to the solvent, as determined from the values of the average O5-C5-C6-O6 torsion angles for each rotamer extracted from each simulation (Table 2). Clearly, idealized values of  $60^\circ$ ,  $180^\circ$ , and  $300^\circ$  are in poor agreement with our averaged solution values. Solvation appears to significantly perturb the value of the  $\omega$  angle in the *tg* rotamer away from the idealized value of  $180^\circ$ .

### NMR analysis

Presented in Tables 3 and 4 are the experimental  $^3J$  values and the rotamer populations for **3** and **6**, respectively, predicted from these values using eqs. [1]–[3] and two sets of limiting  $^3J$  values (32). Unlike the results from the empirically determined limiting  $J$  values (48), the results obtained

**Table 2.** Average  $\omega$  torsion angles from the MD simulations of **3** and **6** in water,  $\text{CH}_2\text{Cl}_2$ , and vacuum.

Environment	<b>3</b>			<b>6</b>		
	<i>gt</i>	<i>tg</i>	<i>gg</i>	<i>gt</i>	<i>tg</i>	<i>gg</i>
H <sub>2</sub> O	70.1	158.3	291.5	70.5	168.6	298.2
$\text{CH}_2\text{Cl}_2$	66.4	161.2	293.7	69.6	170.1	296.3
Vacuum <sup>a</sup>	72.6	171.3	289.4	—	—	—

<sup>a</sup>Calculated using MM3(94) with modified O-C-C-O torsion parameters (27).

with quantum-derived limiting  $J$  values (32) did not result in any nonphysical (negative) rotamer populations. In the case of **3**, regardless of the choice of the methodology, the population of the *tg* rotamer was shown to increase approximately linearly with the decreasing polarity of the small solvent molecules. This observation is consistent with expectations based on gas-phase quantum mechanical calculations of the rotational properties of the  $\omega$  angle in methyl  $\alpha$ -D-glucopyranoside (**23**), which implies that there would be a preferential enhancement of internal hydrogen bonding in low polarity environments, leading, in the limiting case ( $\epsilon = 1$ ), to a population ratio of approximately 43:28:28. In the larger aromatic solvents, the *tg* population is again high, but it does not follow a direct relationship with solvent polarity.

In contrast to **3**, little sensitivity to solvent polarity is displayed by **6**. This is an unexpected result in that quantum

**Table 3.** Experimental  $^3J$  values and rotamer populations for **3**, listed in order of decreasing solvent polarity.

Solvent	Experimental $^3J_{\text{HH}}^a$		Empirical fit (48)			Quantum mechanical fit (32)		
	$^3J_{\text{H5-H6R}}$	$^3J_{\text{H5-H6S}}$	<i>gt</i>	<i>tg</i>	<i>gg</i>	<i>gt</i>	<i>tg</i>	<i>gg</i>
D <sub>2</sub> O	5.44	2.08	51 (49)	-11(0) <sup>b</sup>	60 (51)	48	7	45
DMSO- <i>d</i> <sub>6</sub>	5.87	2.11	55 (53)	-11(0) <sup>b</sup>	56 (47)	53	7	40
CD <sub>3</sub> CN	5.40	2.92	46	0	54	44	16	40
CD <sub>2</sub> Cl <sub>2</sub>	4.87	3.27	39	4	57	37	20	43
CDCl <sub>3</sub>	4.34	3.47	32	7	61	30	22	48
Toluene- <i>d</i> <sub>8</sub>	4.32	3.10	34	3	64	31	18	50
Benzene- <i>d</i> <sub>6</sub>	3.74	2.91	29	0	71	26	16	58

**Note:** Dielectric constants (at 20°): D<sub>2</sub>O (79.8), DMSO (48.9), CH<sub>3</sub>CN (37.5), CH<sub>2</sub>Cl<sub>2</sub> (9.1), CHCl<sub>3</sub> (4.8), toluene (2.4), benzene (2.3) (ref. 51).

<sup>a</sup> $^3J_{\text{HH}}$  from simulated spectra. The maximum error allowed between simulated and experimental spectra was 0.5 Hz.

<sup>b</sup>Values in parentheses were calculated by assuming a zero population for the *tg* rotamer.

**Table 4.** Experimental  $^3J$  values and rotamer populations for **6**.

Solvent	Experimental $^3J_{\text{HH}}^a$		Empirical equation (48)			DFT equation (32)		
	$^3J_{\text{H5-H6R}}$	$^3J_{\text{H5-H6S}}$	<i>gt</i>	<i>tg</i>	<i>gg</i>	<i>gt</i>	<i>tg</i>	<i>gg</i>
D <sub>2</sub> O	7.13	4.30	57	17	27	57	30	12
CD <sub>2</sub> Cl <sub>2</sub>	5.99	5.19	40	29	31	41	40	19
CDCl <sub>3</sub>	6.20	4.24	47	16	36	47	30	23
Toluene- <i>d</i> <sub>8</sub>	6.37	4.88	46	25	30	46	37	17
Benzene- <i>d</i> <sub>6</sub>	6.31	5.22	43	29	28	44	40	16

**Note:** Due to signal overlap, coupling constants could not be measured in DMSO-*d*<sub>6</sub> and CD<sub>3</sub>CN.

<sup>a</sup> $^3J_{\text{HH}}$  from simulated spectra. The maximum error allowed between simulated and experimental spectra was 0.5 Hz.

calculations predict a decrease in polarity should lead to a significant decrease in the population of the *tg* rotamer with an increase in the *gg* (23). This change in population was predicted on the basis of the formation of strong internal hydrogen bonds in the limiting case of a purely apolar environment. However, based on the data in Table 4, it appears that an interpretation of rotamer behavior, based on the view that polar solvents disrupt the internal hydrogen bonds and therefore lead to the rotamer distribution being determined by repulsive 1,3-diaxial electrostatic interactions among O4, O5, and O6, may be correct (23). It should be noted that hydrogen bonds among conformationally restricted 1,3-diaxial hydroxyl groups appear to persist even in water (50).

Overall, the agreement with the predictions from the MD simulations both in terms of the response of the populations to polarity and in quantitative terms is notable. Thus, it is reasonable to probe the simulational results further to extract quantitative information pertaining to the level of intramolecular hydrogen bonding in each rotational state in both water and CH<sub>2</sub>Cl<sub>2</sub>. For each simulation the periods during which hydrogen bonds were present between O4, O5, and O6 were determined for **3** and **6** and are presented in Table 5.

Considerable insight into the sensitivity of internal hydrogen bonding to solvent polarity is provided by the MD data. Some overall trends are apparent; for example, the hydrogen bond between HO6 and O5 is consistently the most occupied (12.9%–18.0%) and the strongest, as indicated by the interoxygen distances. In contrast, hydroxyl group HO4 is consistently a very poor proton donor to HO6 (O4(H)···O6); displaying the lowest occupancies (2.9%–5.8%) and long

internuclear distances is very weak. Similarly, the reverse interaction, that is, one in which HO6 donates a proton to HO4 (O6(H)···O4) is also weak; however, this hydrogen bond shows a strong sensitivity in both **3** and **6** to solvent polarity. In CH<sub>2</sub>Cl<sub>2</sub>, the O4(H)···O6 interaction was predicted to increase both in occupancy and strength. This may be understood given that as a primary alcohol, the proton at O6 is preferentially exposed to solvent and would generally be able to act as either a proton donor or acceptor with water molecules. In the low polarity environment, HO6 has little choice but to interact with either HO4 or HO5. In contrast, HO4 may continue to interact with HO3, regardless of the solvent. Similar arguments may be employed to explain the enhanced strength and occupancy in CH<sub>2</sub>Cl<sub>2</sub> of the O6(H)···O5 hydrogen bond in **3** and **6**. It is notable that CH<sub>2</sub>Cl<sub>2</sub> does not enhance all internal hydrogen bonding to an equal extent. When HO6 acts as a proton donor with O5, the occupancy time for this interaction is approximately doubled in both **3** and **6** in CH<sub>2</sub>Cl<sub>2</sub>. Notably, in the galacto-derivative **6**, the low polarity environment of the CH<sub>2</sub>Cl<sub>2</sub> doubles the occupancy of the O6(H)···O4 hydrogen bond, relative to an aqueous environment, whereas for the gluco-derivative **3**, the occupancy of this hydrogen bond in CH<sub>2</sub>Cl<sub>2</sub> increased nearly fourfold. Therefore, in **6**, although a low polarity environment increases the probability of interactions between O6(H) and O4 and O5, the relative strengths and occupancies of these interactions are unaffected by the solvent. On this basis, it would be predicted that the rotamer populations for **6** would not strongly influenced by solvent polarity, as confirmed by analysis of the NMR data. Since in **3** the O6(H)···O4 hydrogen bond is preferentially favored in

**Table 5.** Average hydrogen bond distances and occupancies for **3** and **6** from the MD data.

MD solvent	Total simulation time (ns)	Molecule	Hydrogen bond		
			O4(H)···O6	O6(H)···O4	O6(H)···O5
Water	122	<b>1</b>	3.41, 3.9	3.39, 4.8	2.98, 18.0
CH <sub>2</sub> Cl <sub>2</sub>	101	<b>1</b>	3.19, 2.9	3.14, 19.0	2.96, 31.4
Water	100	<b>2</b>	3.36, 5.8	3.34, 6.3	3.01, 12.9
CH <sub>2</sub> Cl <sub>2</sub>	114	<b>2</b>	3.36, 2.7	3.35, 12.3	3.00, 26.8

**Note:** Bond distances are between non-hydrogen atoms (in angstroms) and occupancies are presented as a % of total simulation time.

CH<sub>2</sub>Cl<sub>2</sub>, and as it can only form in the *tg* rotamer, a low polarity solvent should induce a shift in rotamer populations in favor of the *tg* state, as confirmed experimentally.

In water, the internal hydrogen bonding networks are disrupted by competition with hydrogen bonds to the solvent. When the internal hydrogen bonds are differentially disrupted, that is, when some become relatively weaker than others, the rotamer populations associated with the  $\omega$  angle may be altered. In the case of **3**, in water the preferential disruption of the O6(H)···O4 interaction destabilized the *tg* rotamer, leading to the observed preference for *gauche* rotamers. In **6**, the O6(H)···O4 hydrogen bond forms most strongly in the *gg* orientation, an orientation in which the O6(H)···O5 hydrogen bond may also form. Thus, in the hydrogen bond strengthening environment of low polarity solvents, a higher ratio of *gg:gt* rotamers would be expected than in water. This trend was observed in the NMR data (see, for example, the ratios 27:57 in D<sub>2</sub>O vs. 36:47 in CDCl<sub>3</sub>). Unlike the case of **3**, the shift in rotamer populations in **6** is less profound, presumably reflecting the fact that the hydrogen bonds in **6** are approximately equally prone to disruption by water.

## Conclusion

The joint NMR and MD analysis of **3** and **6** leads to the conclusion that the balance between inter- and intramolecular interactions involving HO6 plays a direct role in determining the rotational profiles for the  $\omega$  angles. In a low polarity environment, internal hydrogen bonds are shown to be strengthened in both **3** and **6**, however, in **3**, such an environment disproportionately enhances the O6(H)···O4 interaction, leading to an increase in the population of the *tg* state. Without the hydrogen bond enhancement offered by a low polarity environment, both **3** and **6** display rotamer populations that are consistent with expectations based on the minimization of repulsive intramolecular oxygen–oxygen interactions. That is, when in an aqueous environment, the water disrupts stabilizing intramolecular hydrogen bonding and leads to a system whose bond rotational properties are dominated by internal electrostatic repulsions.

The results of this work are generally consistent with the conclusions reached by Rockwell and Grindley (27), to the extent that both studies illustrate that low polarity environments strengthen internal hydrogen bonds in carbohydrates. The data from the MD simulations confirm and quantify the strengthening of the intramolecular hydrogen bonds in CH<sub>2</sub>Cl<sub>2</sub> inferred by the NMR analysis. A significant difference between the two studies pertains to the role of interactions between the solvent and HO6 in glucopyranosides. In

this work, we find that in a low polarity environment HO6 prefers to interact with O4, but that in water these interactions are markedly weakened, indicating that HO6 acts as a hydrogen bond donor to water. That this conclusion was not supported by the studies on methyl 2,3,4-tri-*O*-methyl- $\alpha$ -D-glucopyranoside is perhaps related to the absence of a methyl group at O4 in the present work. It may be that the steric bulk of the methyl groups at the 2-, 3-, and 4-positions detracts from the ability of O4 to act as a hydrogen bond acceptor for HO6. The simulations performed in water have been shown to reproduce the rotamer populations to within experimental error; however, despite the long simulation times, the results from those in CH<sub>2</sub>Cl<sub>2</sub> were less accurate. The MD simulations illustrate that not only are the rotamer populations sensitive to the configuration at C4 in hexopyranosides, but so are the lifetimes and pathways for transitions among the rotameric states. This latter observation indicates that MD simulations of flexible carbohydrates may require very long simulation times (>100 ns) to reach statistical convergence.

## Acknowledgments

This paper is dedicated to Professor W.A. Szarek in honour of his innumerable contributions to carbohydrate chemistry and in recognition of his inspiration as a mentor. We thank the National Institutes of Health (RR05357 and GM55230) for financial support, and JG-O wishes to thank Dr. J. Glushka for helpful discussions regarding the optimization of the NMR experiments.

## References

1. A. Varki. *Glycobiology*, **3**, 97 (1993).
2. R.A. Dwek. *Chem. Rev.* **96**, 683 (1996).
3. H. Lis and N. Sharon. *Chem. Rev.* **98**, 637 (1998).
4. H.C. Joao, I.G. Scragg, and R.A. Dwek. *FEBS Lett.* **307**, 343 (1992).
5. D.F. Wyss, J.S. Choi, J. Li, M.H. Knoppers, K.J. Willis, A.R.N. Arulanandam, A. Smoylar, E.L. Reinherz, and G. Wagner. *Science (Washington, D.C.)*, **269**, 1273 (1995).
6. D.M. Coltart, R.A.K. Royyuru, L.J. Williams, P.W. Glunz, D. Sames, S.D. Kuduk, J.B. Schwarz, X.-T. Chen, S.J. Danishefsky, and D.H. Live. *J. Am. Chem. Soc.* **124**, 9833 (2002).
7. C.J. Bosques, S. Tschampel, R.J. Woods, and B. Imperiali. *J. Am. Chem. Soc.* **126**, 8421 (2004).
8. P.M. Rudd, H.C. Joao, E. Coghill, P. Fiten, M.R. Saunders, G. Opendakker, and R.A. Dwek. *Biochemistry*, **33**, 17 (1994).

9. P.M. Rudd, M.R. Wormald, R.L. Stanfield, M. Huang, N. Mattsson, J.A. Speir, J.A. DiGennaro, J.S. Fetrow, R.A. Dwek, and I.A. Wilson. *J. Mol. Biol.* **293**, 351 (1999).
10. M. Tomana, J. Novak, B.A. Julian, K. Matousovic, K. Konecny, and J. Mestecky. *J. Clinical Investigation*, **104**, 73 (1999).
11. G.J. Davies, V.M.-A. Ducros, A. Varrot, and D.L. Zechel. *Biochem. Soc. Trans.* **31**, 523 (2003).
12. S. Sabesan, S. Neira, and Z. Wasserman. *Carbohydr. Res.* **267**, 239 (1995).
13. Y. Bourne, B. Bolgiano, D.-I. Liao, G. Strecker, P. Cantau, O. Herzberg, T. Feizi, and C. Cambillau. *Nature Struct. Biol.* **1**, 863 (1994).
14. A. Zdanov, Y. Li, D.R. Bundle, S.-J. Deng, C.R. MacKenzie, S.A. Narang, N.M. Young, and M. Cygler. *Proc. Natl. Acad. Sci. U.S.A.* **91**, 6423 (1994).
15. M.R. Wormald, A.J. Petrescu, Y.-L. Pao, A. Glithero, T. Elliot, and R.A. Dwek. *Chem. Rev.* **102**, 371 (2001).
16. J. Jiménez-Barbero and T. Peters. *NMR of glycoconjugates*. Wiley-VCH, Weinheim. 2002.
17. W.A. Bubbs. *Concept. Magn. Res.* **19A**, 1 (2003).
18. D.A. Cumming and J.P. Carver. *Biochemistry*, **26**, 6664 (1987).
19. J. Gonzalez-Outeiriño, R. Kadirvelraj, and R.J. Woods. *Carbohydr. Res.* **340**, 1007 (2005).
20. M. Martín-Pastor, J.L. Asensio, R. López, and J. Jiménez-Barbero. *J. Chem. Soc. Perkin Trans. 2*, 713 (1995).
21. M. Martín-Pastor and C.A. Bush. *Biochemistry*, **39**, 4674 (2000).
22. E.W. Sayers and J.H. Prestegard. *Biophys. J.* **79**, 3313 (2000).
23. K.N. Kirschner and R.J. Woods. *Proc. Natl. Acad. Sci. U.S.A.* **98**, 10541 (2001).
24. H.F. Azurmendi and C.A. Bush. *Carbohydr. Res.* **337**, 905 (2002).
25. R.U. Lemieux and S. Koto. *Tetrahedron*, **30**, 1933 (1974).
26. S. Wolfe, M.-H. Whangbo, and D.J. Mitchell. *Carbohydr. Res.* **69**, 1 (1979).
27. G.D. Rockwell and B.T. Grindley. *J. Am. Chem. Soc.* **120**, 10953 (1998).
28. R.H. Marchessault and S. Perez. *Biopolymers*, **18**, 2369 (1979).
29. K. Bock, and J.Ø. Duus. *J. Carbohydr. Chem.* **13**, 513 (1994).
30. Y. Nishida, H. Hori, H. Ohru, and H. Meguro. *J. Carbohydr. Chem.* **7**, 239 (1988).
31. I. Tvaroska, F.R. Taravel, J.P. Utille, and J. Carver. *Carbohydr. Res.* **337**, 353 (2002).
32. R. Stenutz, I. Carmichael, G. Widmalm, and A.S. Serianni. *J. Org. Chem.* **67**, 949 (2002).
33. N.K. de Vries and H.M. Buck. *Carbohydr. Res.* **165**, 1 (1987).
34. D.A. Cumming and J.P. Carver. *Biochemistry*, **26**, 6676 (1987).
35. K. Yoza, N. Amanokura, Y. Ono, T. Akao, H. Shinmori, H. Takeuchi, S. Shinkai, and D.N. Reinhoudt. *Chem. Eur. J.* **5**, 2722 (1999).
36. R.A. Edington, E.L. Hirst, and E.E. Percival. *J. Chem. Soc.* 2281 (1955).
37. D. Trimmell, W.N. Doane, C.R. Russell, and C.E. Rist. *Carbohydr. Res.* **11**, 497 (1969).
38. D.J. Bell and G.D. Greville. *J. Chem. Soc.* 1136 (1955).
39. D.A. Case, D.A. Pearlman, J.W. Caldwell, T.E. Cheatham III, W.S. Ross, C.S. Simmerling, T.A. Darden, K.M. Merz, R.V. Stanton, A.L. Cheng, J.J. Vincent, M. Crowley, D.M. Ferguson, R.J. Radmer, G.L. Seibel, U.C. Singh, P.K. Weiner, and P.A. Kollman. AMBER 5.0 [computer program]. University of California San Francisco, San Francisco, California. 1997.
40. R.J. Woods, R.A. Dwek, C.J. Edge, and B. Fraser-Reid. *J. Phys. Chem.* **99**, 3832 (1995).
41. W.L. Jorgensen. *J. Am. Chem. Soc.* **103**, 341 (1981).
42. T. Fox and P.A. Kollman. *J. Phys. Chem. B*, **102**, 8070 (1998).
43. K. Marat. SPINWORKS 2.4 [computer program]. Department of Chemistry, University of Manitoba, Winnipeg, Manitoba. 2004
44. PERCH Solutions Ltd. PERCH NMR software [computer program]. PERCH Solutions Ltd., Kuopio, Finland. 2005
45. J.W. Brady. *J. Am. Chem. Soc.* **111**, 5155 (1989).
46. P.J. Hajduk, D.A. Horita, and L.E. Lerner. *J. Am. Chem. Soc.* **115**, 9196 (1993).
47. M. Kraszni, Z. Szakacs, and B. Noszal. *Analyt. Bioanalyt. Chem.* **378**, 1449 (2004).
48. C.A.G. Haasnoot, M. De Leeuw, and C. Altona. *Tetrahedron*, **36**, 2783 (1980).
49. J. Gonzalez-Outeiriño, J. Glushka, A. Siriwardena, and R.J. Woods. *J. Am. Chem. Soc.* **126**, 6866 (2003).
50. J. Hawley, N. Bampos, N. Aboitiz, J. Jiménez-Barbero, M. López de la Paz, J.K.M. Sanders, P. Carmona, and C. Vicent. *Eur. J. Org. Chem.* 1925 (2002).
51. R.C. Weast (*Editor*). *CRC handbook of chemistry and physics*. 59th ed. CRC Press, Inc., Boca Raton, Florida. 1978.